Interaction Notes

Note 539

31. March 1998

Mine Detection with Microwaves

M. Magg
IABG mbH, Ottobrunn, Germany

J. Nitsch
Otto-von-Guericke-Universität Magdeburg, Germany

Abstract

Location and identification of buried land mines is a real challenge for sensor technology and target identification algorithms. We analyse the performance of a bistatic microwave imaging system with a focused synthetic aperture. If the soil is homogeneous and dry with a very smooth surface it will be possible to identify even plastic mines under a 10 cm overburden. However, under a rough surface of wet soil even a relatively big metallic anti-tank mine could be missed, since the signal to clutter ratio gets quite poor under these circumstances.

1. Introduction

Military conflicts left vast tracts of country under the suspicion of contamination by land mines. Efficient, reliable mine detecting, identification and clearing techniques are urgently needed. Buried land mines present a particular hard problem. Standard detection procedures for buried land mines still rely on metal detectors and bayonet probing. Brute force clearing uses deep plowing, moulding and harrowing. Obviously, these procedures can be applied only on limited areas.

The buried mines range from small, inexpensive anti-personal plastic mines with very little metal content to bulky metallic anti-tank mines. Possible mine shapes include disks, cylinders, square boxes and more fancy geometries. The sizes of mines start at about 5 cm and may go up to 40 cm. Looking from above ground, it is virtually impossible to find a unique signature that can be used to discriminate a buried mine from other similar looking pieces of scrap. A low false alarm rate, however, is required for an efficient clearing of expanded lots suspected of mines.

The requirements on civilian mine clearing are quite ambitious:

- Detection rate of 99.9% or better,
- Operating at rough soil surface as well as for wet soil,
- Low false alarm rate, i.e. clear distinction of mines versus scrap, rock pieces, soil surface structures.

It was suggested to exploit the explosive charge which is contained in every mine to detect them under a shallow soil overburden. Almost all explosive charges consist of strongly nitrogenious chemicals. Therefore a high local nitrogen concentration in the soil may indicate a buried mine. The proposals for spotting local nitrogen concentrations close to the soil surface require vaniing technical expenditure. Sniffing by specially trained dogs and γ-ray activation of the natural nitrogen isotop with subsequent detection of the resulting instable isotop are two examples that have been suggested [1].

Another starting point for the detection and identification of buried mines hopes to exploit the casing geometry of buried mines as seen by microwaves. An aspect independent way of perceiving the geometry of a target is given by the complex frequency poles of the electromagnetic scattering amplitude caused by a buried target if it gets illuminated by microwaves [2]. If one has a catalogue of these complex frequency pole patterns for all interesting buried targets one may hope to determine the target from an analysis of microwave scattering data in the relevant frequency band.

One diffculty with this method when applied to targets buried in the soil is the vaniing influence of the soil overburden on the received scattering signal. This is in contrast to the better known application of this identification technique to airborne targets. The influence of the air on the back scattering data is much smaller and reasonably well under control. The effect of soil on the comlex resonance frequencies of a buried target varies with the thickness and composition of the soil overburden. Furthermore in the S-band, which is most relevant for mine identification, wet soil is expected to produce a strong signal dispersion, which may disturb the final complex pole analysis of the scattering data.

In this paper we analyse narrow band microwave imaging of buried objects as inspired by much employed high resolution radar techniques [3,4]. The objective is to investigate the performance of microwave imaging for mine searching and identification, exhausting the physical capabilties of microwaves without caring much about implementation details.

2. Bistatic Microwave Imaging with Focussing Synthetic Aperture

In order to obtain a good spatial resolution for buried targets the wave length used for microwave imaging should be chosen as small as possible. Since a mine buried under a 20 cm thick layer of moderately wet soil should be still visible, the microwave should be able to cross a 1 cm layer of water without too much absorption. Looking at the absorption coefficient of water as a function of frequency one learns, that one cannot go beyond S-band frequencies. Therefore spatial resolution for ground penetrating imaging systems based on non-ionizing electromagnetic waves cannot go much below 4 to 6 cm. All numerical studies in this paper use a frequency of 3.5 GHz.

In order to look into the soil one has to overcome the reflection from the soil surface which is superimposed to the scattering echos from buried objects. For vertical illumination a soil surface produces a reflection factor r , given by:

$$r = (n-1)/(n+1), \tag{1}$$

where n is the index of refraction of the soil. This means for n = 3 half of the incident wave amplitude would be reflected at the ground surface and would interfere with the echo from buried objects. Since the radar range resolution is not sufficient to separate the ground surface echo from that of shallowly buried targets, suppression of the ground surface echo is required.

The reflection from a plane surface is minimal (ideally zero) if the plane is illuminated along the Brewster direction by a wave which is polarized in the plane of incidence. The Brewster angle is determined by the index of refraction of the soil:

$$\tan\theta_B = n \tag{2}$$

For soil this angle lays in the range from 52° to 85°. If the illumination misses the Brewster angle by 3° the reflection factor will be still less than 10%.

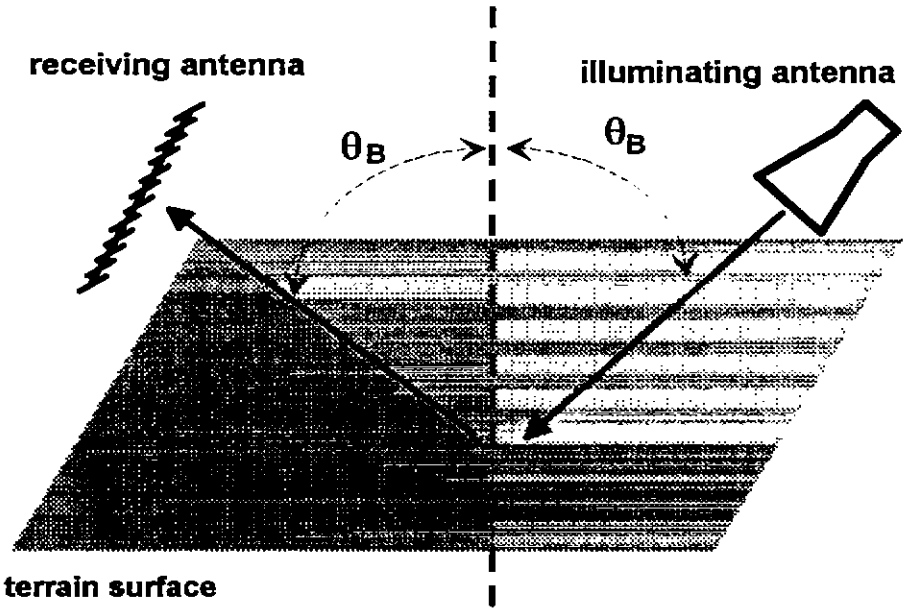

Fig. 1: Bistatic microwave mine detection and imaging system

The spatial resolution increases with the aperture dimension of the receiving antenna and decreases with the distance from the antenna to the focussed region. Hence, in order to

achieve a high resolution power for the microwave imaging system the receiving aperture should be as close to ground as possible. Practical operation conditions require a sufficient terrain clearance. In our study we assume that the receiving antenna is 0.7 m above average ground level. The receiving antenna is designed as an approximately 1 m long linear dipole array. A much bigger array would restrict the possible use of the mine searching system which could be mounted in front of a small cross-country vehicle.

The resolution in the direction orthogonal to the linear array is produced by the forward move of the complete imaging system. The receiving array sweeps a two dimensional ground strip, thereby forming a synthetic aperture, much like in a forward looking SAR-system. At every step, the received complex scattering amplitude as seen by the individual dipole elements of the receiving array will be stored in the memory of a data processing unit.
The stepping direction will be called 'longitudinal' whereas the orthogonal direction, parallel to the linear receiving antenna, will be addressed as 'lateral'.
The longitudinal length of the synthetic aperture, i.e. the number of real antenna positions used to compose an image of a point in real space determines the resolution of the system in the longitudinal direction. The physical length of the array, i.e. the lateral width of the synthetic apertur controls the lateral resolution.
Since the microwave scattering is concentrated around the reflection angle, an aperture length in stepping direction of the order of 1 m would be sufficient. Larger aperture dimension would improve only marginally the resolution power of the system at the expense of a longer image processing time.

Figure 1 illustrates the basic system design. Illuminating and receiving antenna are kept at a riggid horizontal distance from each other. In our study this distance is 2 m. The complete system steps forward in the direction from the receiving array to the illuminating horn. The receiving array is oriented laterally. The horn and the dipole elements of the receiving array both are inclined by angle θ_B against the vertical.

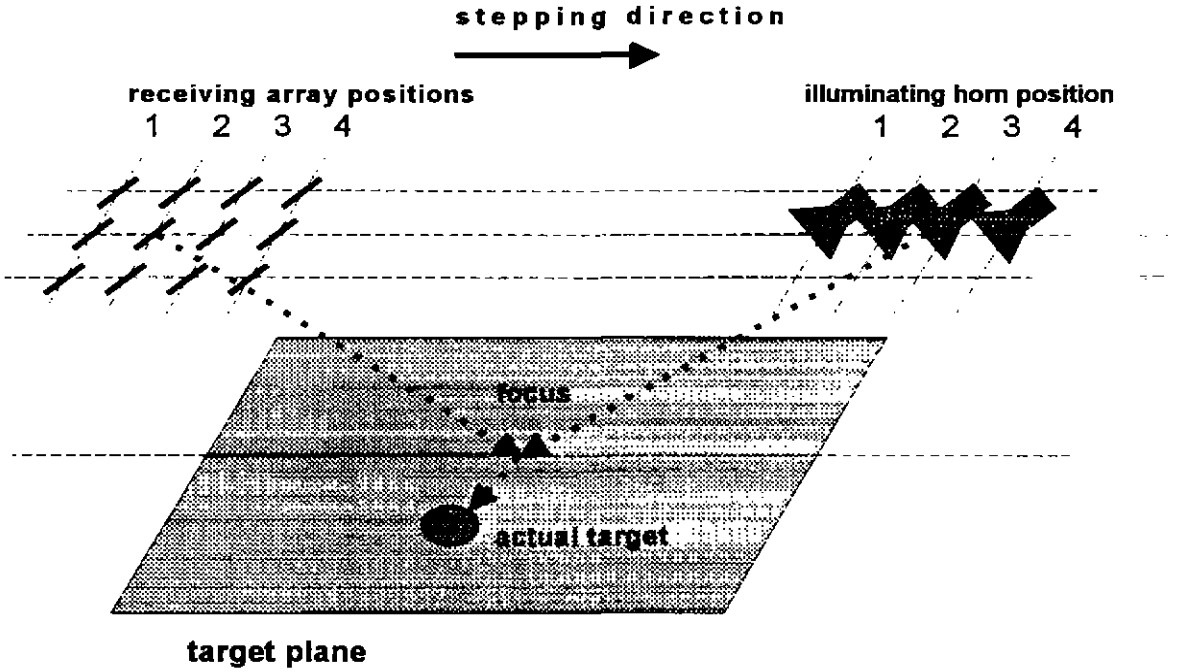

Fig.2: Synthetic aperture with 4 real antenna positions.

Figure 2 sketches the bistatic system in action, forming a synthetic plane aperture which consists out of 4 real antenna positions.

3. Longitudinal and Lateral Resolution Power

The processing of the stored scattering data consists in focussing the data relative to a grid of focus points which is projected onto the presumed mine laying plane (target plane). For a chosen focus point in the target plane one calculates the optical path length from the illuminating antenna via that focus point to the individual antenna elements in the receiving aperture. The complex scattering amplitudes as actuallly received by the elements of the synthetic aperture get multiplied by the complex conjugate phases related to the path length from illuminating antenna to receiving element via the chosen focal point on the target plane. The resulting phase corrected amplitudes are summed over all elements of the synthetic aperture. For a target that sits directly at a focus point all phase-corrected amplitudes of the individual elements in the synthetic aperture add up whereas the phase-corrected elementwise scattering amplitudes of a target which is more than a resolution distance away from that focus point would cancel each other almost completely in the summed antenna response.

This focussing is performed one by one for all focus points of the grid. By mapping the distribution of the focussed antenna response onto the target plane one obtains an image of all scattering objects which are buried within a certain layer around the target plane. The thickness of this layer is determined formally by the depth of fields of the imaging system. As we shall see later it is not the formal depth field but the much shorter electromagnetic penetration depth which puts actually the limit for the vision into the soil.

Mathematically the focussing algorithm is defined as follows. Let $A(m,n)$ be the complex scattering amplitude as actually received by the m-th array element of the array at the n-th step position over the target plane. Furthermore let (x,y) be the coordinates of a chosen focus point on the target plane. Then the total amplitude received by the focussed aperture is given by:

$$A_f(x,y) = \sum_{m,n} A(m,n) \cdot \exp\{-j \cdot k \cdot [\sqrt{h^2 + (x_n - x)^2 + (y_m - y)^2} + \sqrt{h^2 + (x_n + 2a - x)^2}]\} \qquad (3)$$

h distance of the target plane from the aperture plane,
k wave vector $2\pi \cdot f / c$ (f = frequency, c = speeed of light)
a half distance between illuminatinig hom and receiving linear array,
x_n longitudinal position of the receiving antenna at the n-th step,
y_m lateral distance of the m-th array element from array line center.

The height h and the distance a are related by the incident angle:

$$\cot\theta_B = h / a \quad . \qquad (4)$$

The focussing is achieved by compensating the phases as actually received by the different antenna elements by the path lengths of the ray pencil which passes the chosen focus point.

The summation in (3) runs over all elements m of the real linear array and all positions n which form the synthetic aperture. Note that the focus point belongs to the Fresnel region of the receiving antenna. The distance from the receiving antenna to the focus point is not much larger than the longitudinal and lateral aperture dimension.

The formula (3) neglects the fact, that the focus point is below ground. The correct electromagnetic path from transmitting horn to receiving array antenna via focus point would have to take refraction into account. For a shallow overburden this would cause a small path length correction. In the numerical simulation, which we report later on, the full 'optical' path length has been computed and used for the focussing. Unfortunately the explicit expression for the full optical path length is somewhat bulky to write down explicitely, therefore we stay with the deputy formula (3).

One may estimate the spatial resolution of the synthetic aperture following a popular $\lambda/2$-argument in optics and antenna theory:

First compute the path length for the so-called central ray. The central ray starts at the wave source, scatters off the target point and ends at the centre of the receiving aperture. Next compute the path length for the so-called boundary ray. The boundary ray shares with the central ray the same starting and scattering points but it ends at the boundary of the receiving aperture. If both path lengths differ by half a wavelength, then the scattering signal caused by that target point cancels in the received total antenna signal.

For a focussed array antenna it is the relative path length which enters the preceeding argument. The relative path length is obtained from the original path length by subtracting from it the length of the focus reference path. The focus reference path has the same starting and end points as the original central ray, resp. boundary ray, however, it passes through the focus point instead of being scattered off at the target point.

According to the $\lambda/2$ argument a target point close to a chosen focus point will not contribute significantly to the signal received from that focus point, if the relative path lengths for the central and the boundary ray via that target point differ by half a wavelength or more.

Figure 3 displays the rays which are relevant for the estimation whether a point T contributes to the image of an object at the focus point F or not.

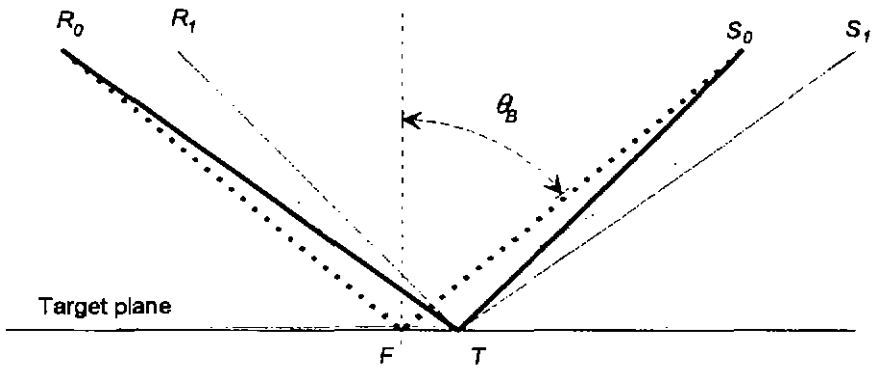

Fig.3: Cut in longitudinal direction: central and boundary rays of the synthetic aperture; R_0 and R_1 central and boundary receiver antenna position, respectively, S_0 and S_1 source central and boundary source position, respectively, T target position , F focus position

Here and in the figures below we distinguish the rays types by the convention:

central rays	→ fat lines,
boundary rays	→ normal lines,
rays scattered at the target	→ solid lines,
reference rays passing the focus	→ broken lines.

The distances $\overline{R_0 R_1}$ and $\overline{S_0 S_1}$ are both equal to half of the longitudinal dimension L of the synthetic aperture. Let x denote the distance from the target T to the chosen focus F. The horizontal distance between the receiver array and illuminating horn is $2a$. Following Figure 3 one identifies $\overline{R_0 T} + \overline{T S_0}$ as the path length for the central ray scattered at the target, similarly $\overline{R_0 F} + \overline{F S_0}$ is the path length for the associated reference ray. The length of the boundary ray scattered at the target is $\overline{R_1 T} + \overline{T S_1}$, and finally $\overline{R_1 F} + \overline{F S_1}$ is the path length for the reference ray associated with the boundary ray.

The path length difference between the signals received by the boundary element and the central element both focussed relative to point F is composed as follows:

$$W(x) = \overline{R_0 T} + \overline{T S_0} - \overline{R_0 F} - \overline{F S_0} - \overline{R_1 T} - \overline{T S_1} + \overline{R_1 F} + \overline{F S_1}$$

In linear approximation for x this path length difference becomes:

$$W(x) \approx \frac{x \cdot L}{\sqrt{h^2 + a^2}} \cdot \left[\frac{h^2}{a^2 + h^2} + \frac{L^2}{8} \cdot \frac{5a^2 - h^2}{(a^2 + h^2)^2} \right] \qquad (5)$$

The factor which multiplies the distance x in equation (5) corresponds to the 'numerical aperture' in optics. For a rough estimate one may neclect non-linear corrections in the longitudinal aperture dimension L. The contribution of the target point to the signal as received by the synthetic aperture focussed at point F vanishes if the path length difference W is equal to half a wave length λ. This gives an estimate of the smallest longitudinal scale x_{min} which can be resolved by the the bistatic synthetic focused aperture system:

$$x_{\min} \approx \tfrac{1}{2} \cdot \lambda \cdot \sqrt{h^2 + a^2} \,/\, (L \cdot \cos^2 \theta_B) \qquad (6)$$

Except for an additional $\cos\theta_B$ factor in the denominator, this is just what is known from synthetic apertures used in radar applications. Note the factor 1/2 which is a bonus not valid for real apertures.

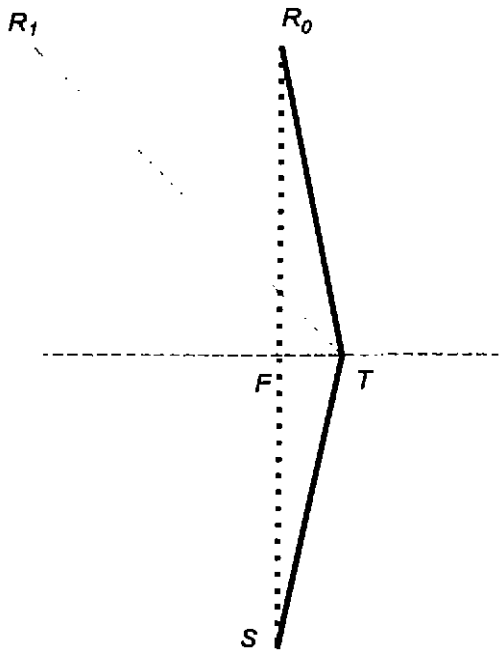

Fig. 4: Lateral direction: central and boundary rays of the bistatic imaging system; R_0 and R_1 central and boundary receiver array element, respectively, S position of the illuminating source.

In the lateral direction the synthetic aperture is actually a real aperture given by the length of the receiving array line. Figure 4 sketches the ray geometry as seen from above.

The linear receiving array antenna has a length $2B$. The relevant distance scales in Figure 4 are:

$$\overline{R_1 R_0} = \tfrac{1}{2}B; \quad \overline{R_0 F} = \overline{F S} = \sqrt{a^2 + h^2}; \quad \overline{F T} = y. \tag{7}$$

Remember that R_1 and R_0 keep a distance h to the target plane. The focus point F and the target point T lay in that target plane.

The path length difference between the signal received by the lateral boundary element and the central element both focussed relative to point F one obtains:

$$W(y) = \overline{R_0 T} + \overline{T S} - \overline{R_0 F} - \overline{F S} - \overline{R_1 T} - \overline{T S} + \overline{R_1 F} + \overline{F S}$$

The source position cancels exactly in the path length difference. Up to non-linear terms in the lateral target distance from the focus point one gets:

$$W(y) \approx y \cdot B / (2\sqrt{a^2 + h^2 + \tfrac{1}{4}B^2}) \quad . \tag{8}$$

The analogous reasoning as for the longitudinal case implies a lateral resolution:

$$y_{min} \approx \lambda \cdot \sqrt{a^2 + h^2} / B. \tag{9}$$

Non-linear contributions of the lateral apertur dimension B have been ignored in this estimate.

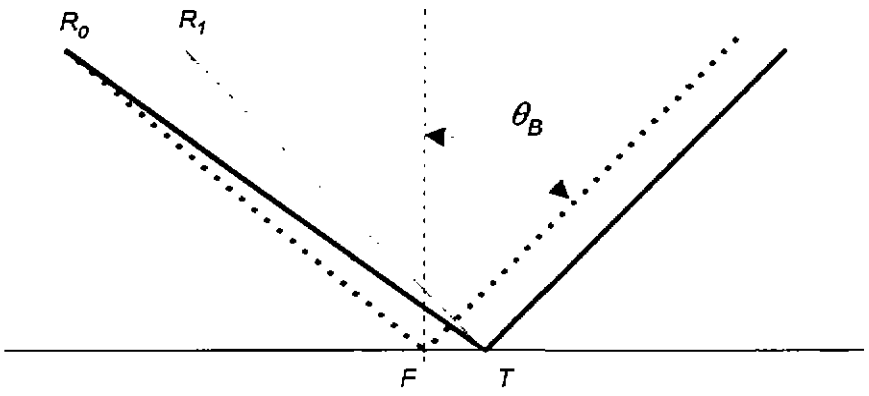

Fig. 5: Longitudinal direction: central and boundary rays in the synthetic aperture; the illumination is by a remote spatially fixed source. R_0 receiver antenna central position, R_1 receiver antenna boundary position, T Target point , F focus point

The lateral resolution changes if the illumination occurs by a spatially fixed transmitting antenna, i.e., if the horn antenna does not follow the forward stepping of the receiving array. Figure 5 shows the situation if the ground gets illuminated by a remote spatially fixed transmitting antenna.

In this environment the path length difference between the signal received by the lateral boundary element and the central element both focussed relative to point F is:

$$W(x) \approx \frac{1}{2} \cdot \frac{x \cdot L}{\sqrt{h^2 + a^2}} \cdot \frac{h^2}{a^2 + h^2} \cdot \left[1 - \frac{3}{4} \cdot \frac{a \cdot L}{a^2 + h^2} \right]. \tag{10}$$

This leads to the following estimate for the longitudinal resolution:

$$x_{\min} \approx \lambda \cdot \sqrt{a^2 + h^2} \,/ (L \cdot \cos^2 \theta_B) \ , \tag{11}$$

This is twice as coarse as what is obtained with the comoving illuminating antenna.

Finally the depth of fields for the bistatic imaging system has to be determined. If the receiving antenna focusses at objects in a chosen target plane (parallel to the ground surface) it displays also objects which lay somewhat above or below that target plane. The depth range for which targets are reasonably well mapped by the bistatic imaging system (while focussing at a chosen target depth) is the 'depth of fields'.

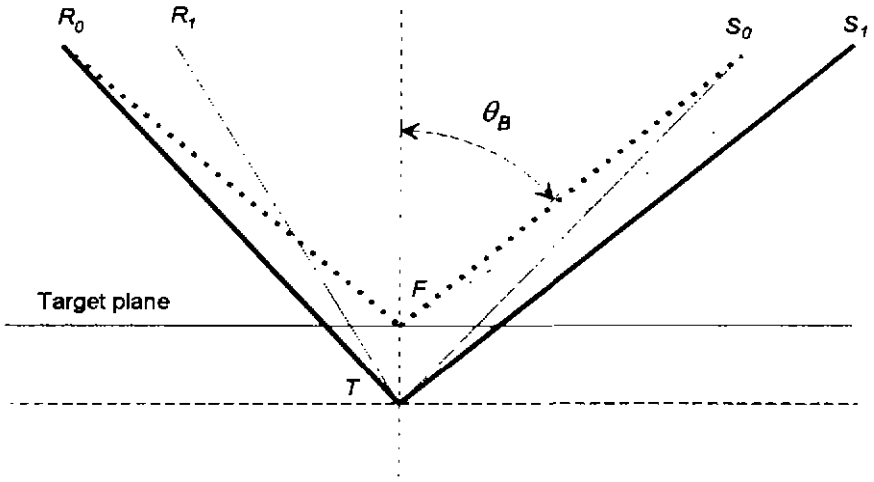

Fig.6: Depth of fields: central and boundary rays for a synthetic aperture; actual target T is below focus point F.

Figure 6 shows the central rays and the boundary rays for a target point laying in a different depth than the chosen focus.

If the antenna is focussed at point F and the scattering occurs at target T, then the path length difference becomes:

$$W(z) = \overline{R_1\,T} + \overline{T\,S_1} - \overline{R_1\,F} - \overline{F\,S_1} - \overline{R_0\,T} - \overline{T\,S_0} + \overline{R_0\,F} + \overline{F\,S_0}$$

The distance $\overline{F\,T}$ of the actual target from the assumed target plane is called z. Keeping only linear terms in z one finds:

$$W(z) = h \cdot z \cdot [1/\sqrt{(a+\tfrac{1}{2}L)^2 + h^2} + 1/\sqrt{(a-\tfrac{1}{2}L)^2 + h^2} - 2/\sqrt{a^2+h^2}]. \qquad (12)$$

Neglecting quartic and higher terms in the longitudinal aperture dimension L one gets:

$$W(z) \approx \frac{z}{4} \cdot \frac{L^2}{a^2+h^2} \cdot \cos\theta_B \cdot [2 - 3\cos^2\theta_B] \qquad (13)$$

The contribution of an actual target to the assumed target plane can be ignored, if the distance of the actual target to that plane is larger than:

$$z_{min} \approx 2\lambda \cdot (h^2 + a^2) / [L^2 \cdot \cos\theta_B \cdot (2 - 3\cos^2\theta_B)]. \qquad (14)$$

This results expresses the limits of the depth of field which are due to the longitudinal aperture dimension L. The lateral aperture dimension B causes a slightly different bound for the depth of field:

$$z_{min} \approx 4\lambda \cdot (h^2 + a^2) / (B^2 \cdot \cos\theta_B) \qquad (15)$$

Actually the formal depth of field is not particularly relevant for a ground penetrating microwave system. In general the penetration depth of 3.5 GHz microwaves in soil is much shorter ($\approx 3\,\lambda$) than the formal depth of field which was estimated by eqs. (13) and (14).

Figure 7 shows the calculated intensity distribution caused by a single pointlike target as seen by a bistatic imaging sytem focussed at the target plane. The intensity is given by

the modulus squared of the amplitude in eq. (3). The pointlike target is modelled as an isotropical scattering center in the target plane at coordinates (x', y') which gets illuminated by a comoving transmitting antenna at a horizontal distance $2a$ from the receiving array line position x_n:

$$A(m,n) = \exp\{j \cdot k \cdot [\sqrt{h^2 + (x_n - x')^2 + (y_m - y')^2} + \sqrt{h^2 + (x_n + 2a - x')^2}]\} \qquad (16)$$

No approximations have been made in the evaluations of the square roots.

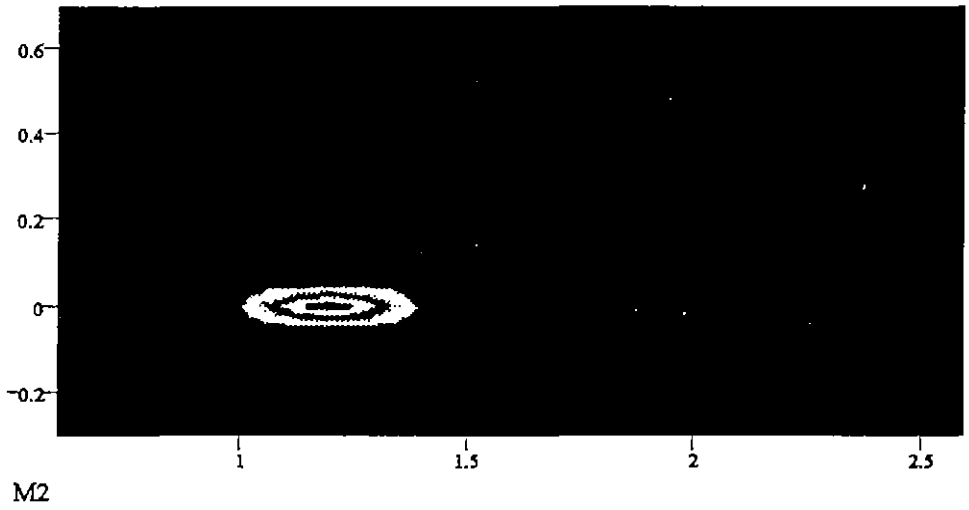

Fig. 7: Image of a pointlike target at position (1.2,0) in the target plane, 0.75 m below the aperture plane of a bistatic synthetic aperture imaging system, illuminating antenna moves together with the receiving array.

The longitudinal resolution shown is about 0.3 m, whereas the lateral resolution is 0.06 m. According to the eqs. (6) and (9), an aperture size of 40 cm by 120 cm allows a resolution of 48 cm by 9 cm (longitudinal by lateral), at a target plane 0.75 m below the receiving array.

Consider now a bistatic system where the illuminating horn remains fixed while the receiving array is sweeping the synthetic aperture. If the illuminating horn is not too close to the surface, the illumination can be modelled as a portion of a plane wave incident on the surface under the angle θ_B. One obtains an expression similar to equation (3) for the total amplitude received by the focussed aperture of that system. The elementwise received amplitudes now take the form:

$$A(m,n) = \exp\{j \cdot k \cdot [\sqrt{h^2 + (x_n - x')^2 + (y_m - y')^2} - x' \cdot \sin\theta_B]\} \qquad (17)$$

The focussing phase shift is

$$\exp\{-j \cdot k \cdot [\sqrt{h^2 + (x_n - x')^2 + (y_m - y')^2} - x' \cdot \sin\theta_B]\} \qquad (18)$$

The intensity received by this system design from the same pointlike target is now displayed in Figure 8. Note that the longitudinal resolution is now at least twice as coarse as for the system with comoving illumination. This behaviour is predicted by eq. (11) as compared to eq. (6).

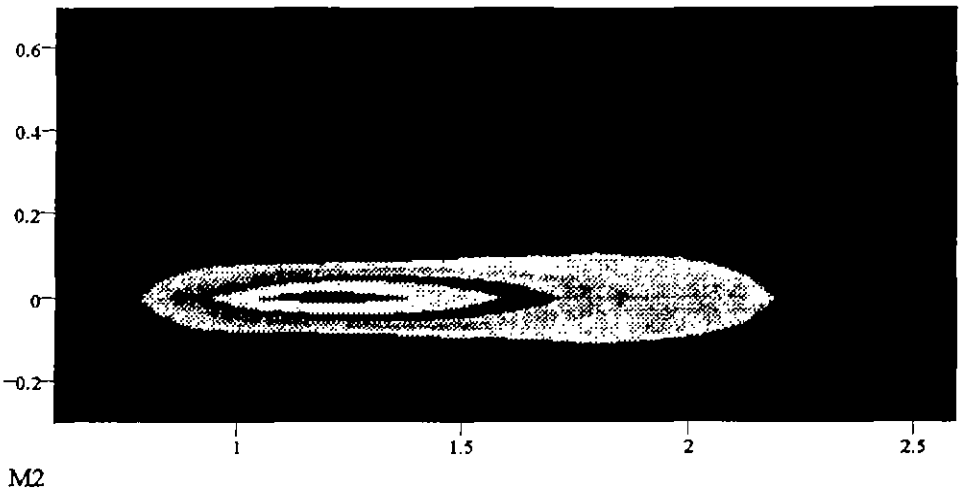

Fig. 8: Image of a pointlike target at position (1.2,0) in the target plane 0.75 m below the aperture plane of a bistatic synthetic aperture imaging system; the illuminating antenna is spatially fixed

The analysis of resolution power was based solely on the array pattern characteristics. The directional pattern of the individual elements in the receiving antenna array was not taken into account. Furthermore the isotropic scatterer model of the buried target is a severe over-simplification. The bistatic scattering cross-section of a buried target tends to concentrate the scattering field around the reflection direction. Both directional gains would reduce the aperture dimensions which are required in order to obtain a desired resolution.

4. Signal to Clutter Ratio

As important as the resolution power is the targets contrast relative to the background for the imaging device. Since an ideally flat ground surface would cause no reflection the background is produced solely by surface structures and inhomogeneities in the soil. To get a feeling for realistic signal to clutter ratios when the bistatic imaging system is applied to mine searching, we display first the signals of mine-like objects buried under an ideal overburden, e.g. homogeneous sand with a smoothly raked surface. Next we compare this ideal case with the image produced by a distinctively structured soil surface without any buried mines.

4.1 Scattered Fields of Buried Mines and of Soil Surface Structures

In this paragraph we display the scattering fields which are caused by various buried targets and soil surfaces when the surface gets illuminated by an incident plane wave. The incident angle for the illumination is always $\theta_B = 58°$. The incident field is normalized to 1 V/m, the frequency is 3.5 GHz.

The scattering fields are obtained by employing numerical simulation method as provided by a well established finite differences time domain code [5]. Two types of soil are investigated:

- very dry sand with dielectric constant $\varepsilon'=2.55$ and specific conductivity $\kappa=0.001$ S/m ,
- wet clay with dielectric constant $\varepsilon'=10$ and specific conductivity $\kappa=0.1$ S/m.

For both soil types inhomogeneities are not included in the model. However, the model for the plastic mine also may be taken as a hint of the kind of echo that is to be expected from a natural inhomogeneity in the soil. The mine models are buried under a 10 cm deep uniform soil layer. The scattered fields are plotted in the plane of incidence and in a horizontal cut 0.65 m above average ground level. The horizontal plot displays only one half of the scattering field which is symmetric relative to the incident plane, since all targets in this study have this symmetry and the polarisation is parallel to the incident plane.

The contour plots (Figs. 9 and 10 to 15) linearly map the intensity of the scattered field into gray values. White corresponds to the maximum intensity, black to zero intensity. The scales at the plot axis state the longitudinal, the vertical and the lateral distances in meter. The mines are indicated in the incident plane plots, close to longitudinal coordinate 0. The plots display the scattered fields only, the incident field coming from top right has been filtered out. The concentration of the scattering in the reflection direction is clearly visible. Due to available computer resources the modelled soil layer was limited to 0.5 m in depth. For the dry sand this is somewhat less than what is desirable. Therefore the displayed field distribution in the lower part of the dry sand layer has to be taken with some care. The scattered field in the airspace, however, is believed to be simulated reliably.

[illegible]	field (V/m)
metallic anti-tank mine in dry sand	0.23
big plastic mine in dry sand	0.065
rough terrain surface in dry sand	0.35
square metallic mine in dry sand	0.055
metallic anti-tank mine in wet clay	0.038
rough terrain surface in wet clay	0.35

Tab. 1: Peak values of scattered fields at 0.65 m above ground level

Table 1 summarizes the peak values of the microwave scattering signals as seen by a probe 0.65 m above average ground level for the scattering objects which have been examined in this study.

The modelling data of the employed mine types are as follows:

metallic anti-tank mine: cylinder, ∅ 24 cm, height 8 cm, ideally conducting
big dielectric mine: cylinder, ∅ 24 cm, height 8 cm, non-conducting, $\varepsilon'= 3.7$
metallic square mine: 10 cm squared, height 4 cm, ideally conducting

The modelling of the rough surface is represented in Figure 11. The displayed surface segment is 3 m long.

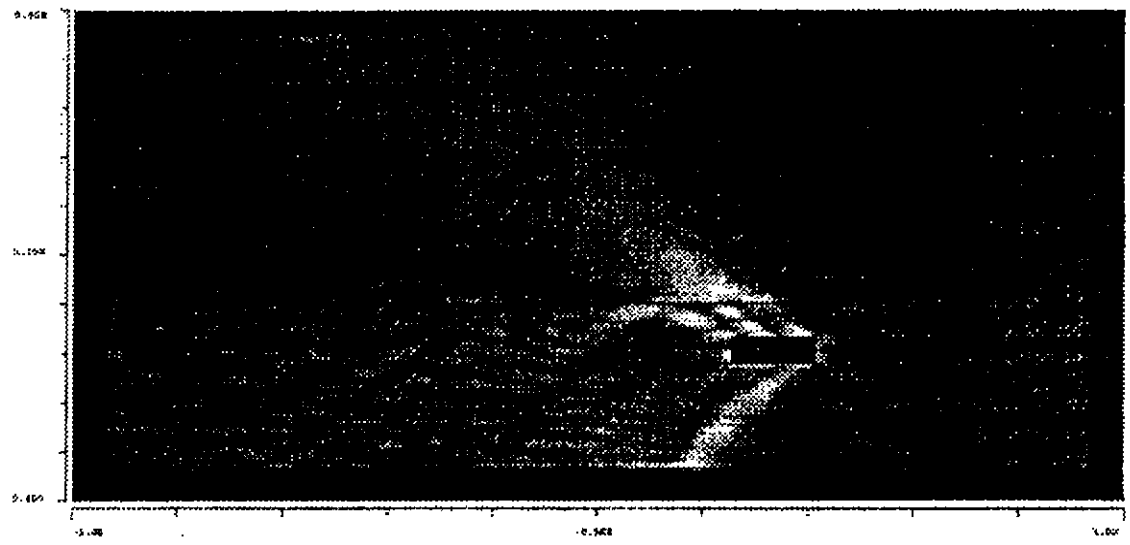

(a) max=1.2 V/m

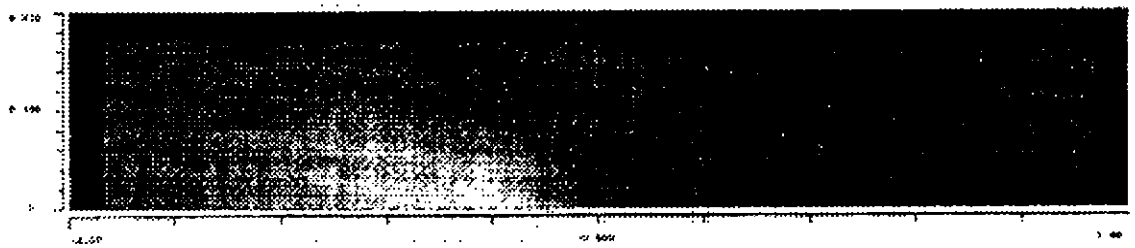

(b) max=0.26 V/m

Fig. 9: Scattered field produced by a metallic cylindrical mine, ∅ 24 cm, height 8 cm buried in dry sand; (a) incidence plane, (b) horizontal plane.

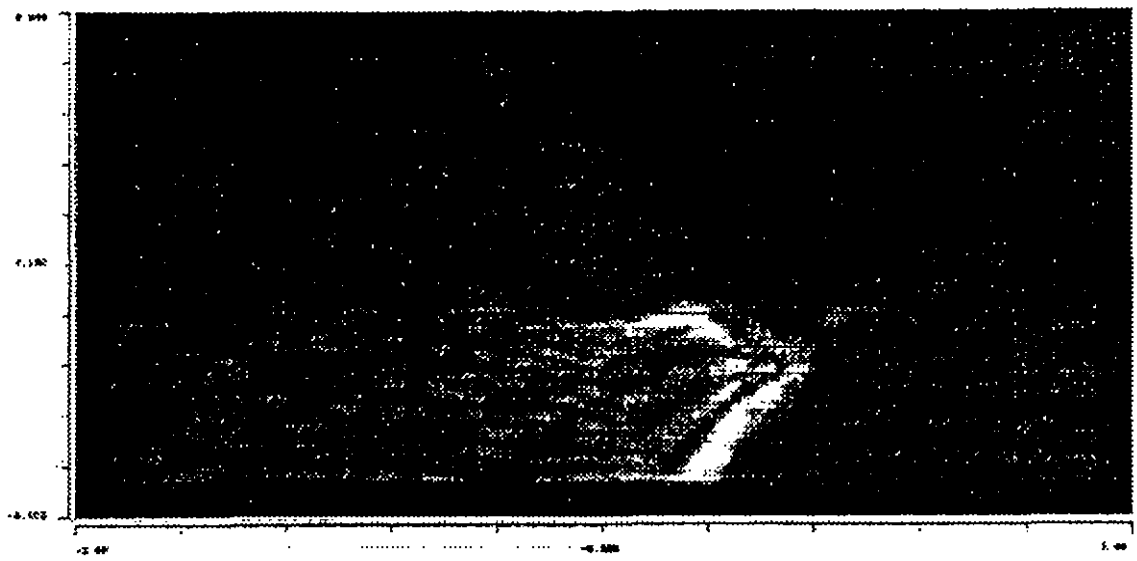

(a) max=1.8 V/m

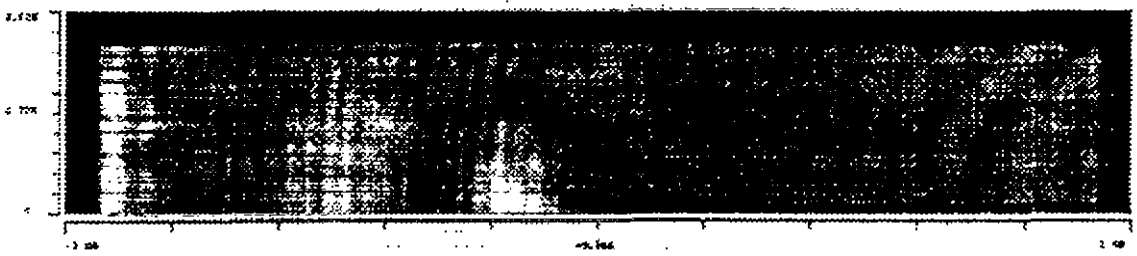

(b) max=0.072 V/m

Fig. 10: Scattered field produced by a dielectric cylindrical mine, ∅ 24 cm, height 8 cm, ε'=3.70, buried in dry sand; (a) incidence plane, (b) horizontal plane

Fig. 11: Coputer modell of a rough terrain surface with sharp relief structures ±5 cm.

(a) max=2.8 V/m

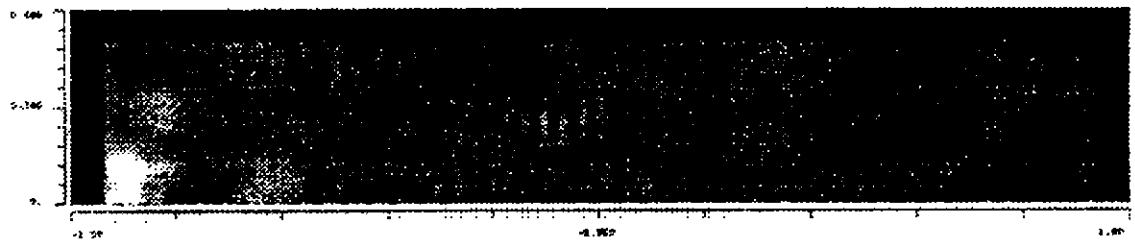

(b) max=0.6 V/m

Fig. 12: Scattered field produced by a rough terrain surface in dry sand; (a) incidence plane, (b) horizontal plane

(a) max=0.76 V/m

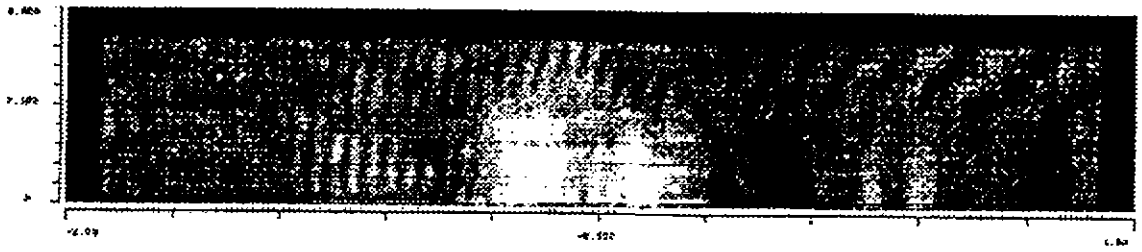

(b) max=0.06 V/m

Fig. 13: Scattering field produced by metallic 10 cm square mine, height 4 cm buried in dry sand; (a) incidence plane, (b) horizontal plane

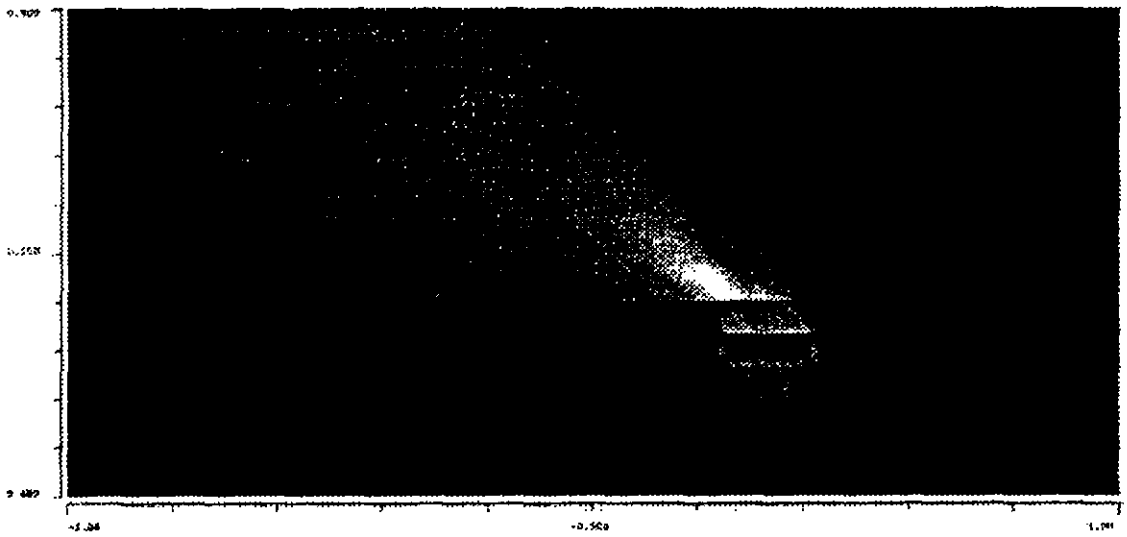

(a) max=0.18 V/m

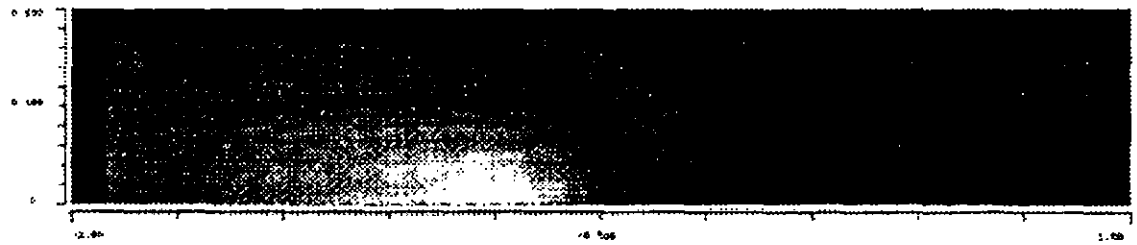

(b) max=0.04 V/m

Fig. 14: Scattered field produced by a metallic cylindrical mine, ∅ 24 cm, height 8 cm buried in wet clay; (a) incidence plane, (b) horizontal plane

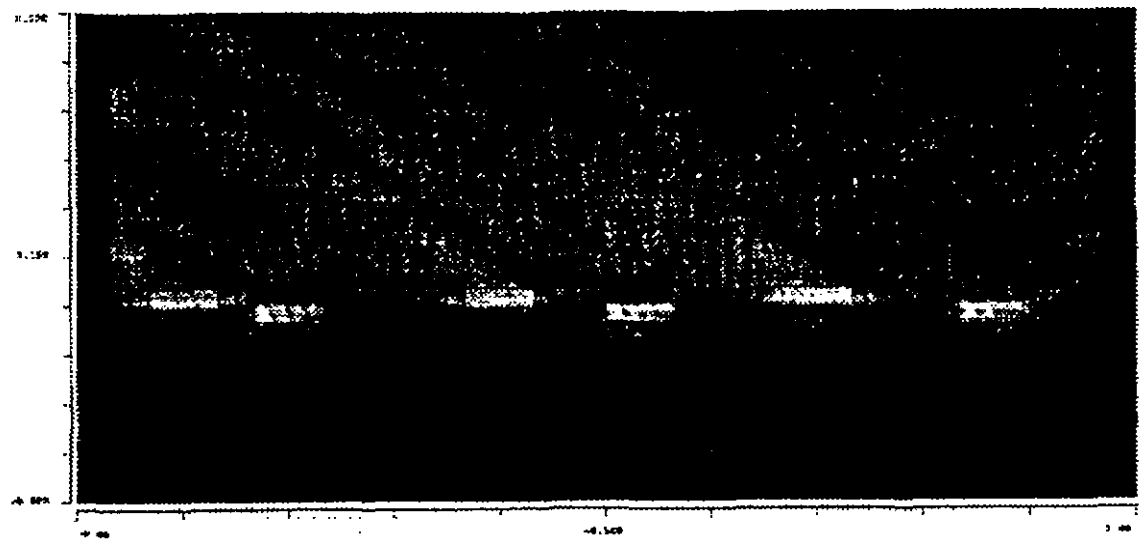

(a) max=1.4 V/m

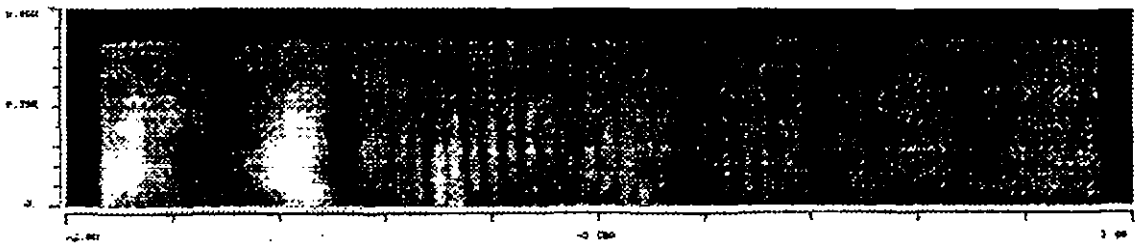

(b) max=0.45 V/m

Fig. 15: Scattering field produced by a rough terrain surface in wet clay; (a) incidence plane, (b) horizontal plane

4.2 Microwave Images of Buried Mines and of Soil Surface Structures

The scattered field as displayed in the previous section is the input data for the computational image formation as outlined in Section 3. Note that in the numerical simulation the illumination was mounted at a fixed position in space during the recording of the scattered field. The reason for this set-up was purely technical: It is much cheaper (i.e. faster) to simulate a spatially fixed illumination, since it requires the computation of just one scattered field configuration. The original bistatic, synthetic aperture imaging system uses a comoving illuminating horn antenna. This implies for every single step forward a separate computation of the scattered field, even though this field is evaluated only at the corresponding position of the receiving array elements.

For the signal to clutter ratio the two different methods are expected to give the same results. As to the resolution power it was argued in Section 3 , that the spatially fixed illumination needs a longitudinal aperture roughly twice as large as the comoving illumination in order to produce the same longitudinal resolution. The images in this section are obtained with the following aperture dimensions: 0.8 m lateral, 0.32 m longitudinal.

To evaluate the following images of targets as produced by the studied bistatic imaging system-design one has to refer to the gray values scales given on the left side of the plots. The contrast produced by the metallic anti-tank mine is almost 6-times stronger than that of the big plastic mine. Comparing the gray values of the mine models with those of the surface models one may predict a signal to clutter ratio for the imaging of mine-like targets achieveable within the considered system-design. As one learns from a glance at Tab. 2. even for dry sand the results do not look too promising. Of course, one cannot discuss the identification capability solely on the basis of the global signal to clutter ratio. Preknowledge on the mine shapes would help to discriminate clutter against a real mine target if the resolution power of the imaging is good enough. Unfortunately, a resolution of 5 cm seems not sufficient to support pattern recognition methods in mine identification.

metallic anti-tank mine	1.26
big plastic mine	0.22
square metallic mine	0.21

Tab. 2: Signal to clutter ratio for targets buried in dry sand under a surface with sharp relief structures

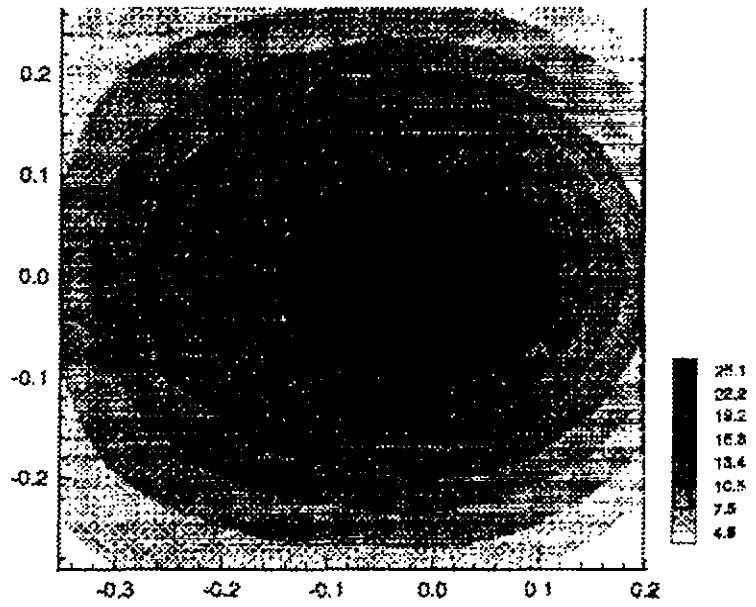

Fig. 16: Image produced by a metallic cylindrical mine ∅ 24 cm, height 8 cm, buried in dry sand

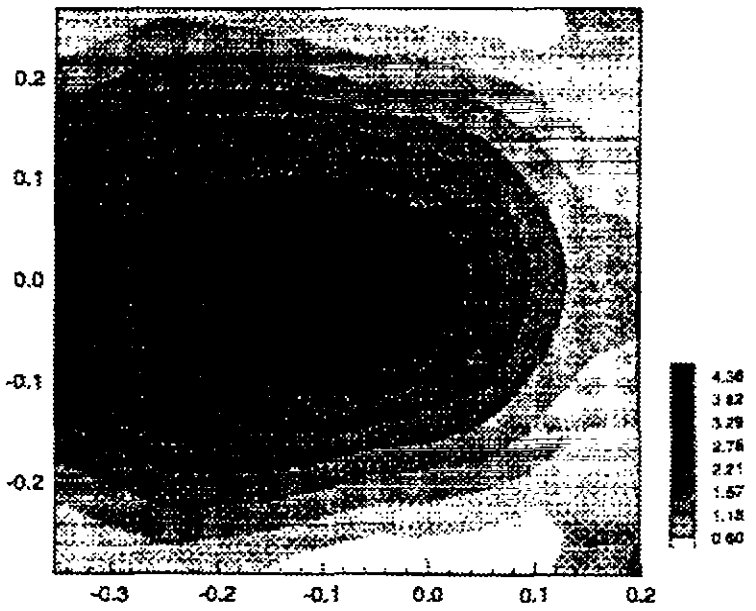

Fig. 17: Image produced by a dielectric cylindrical mine ∅ 24 cm, height 8 cm, buried in dry sand

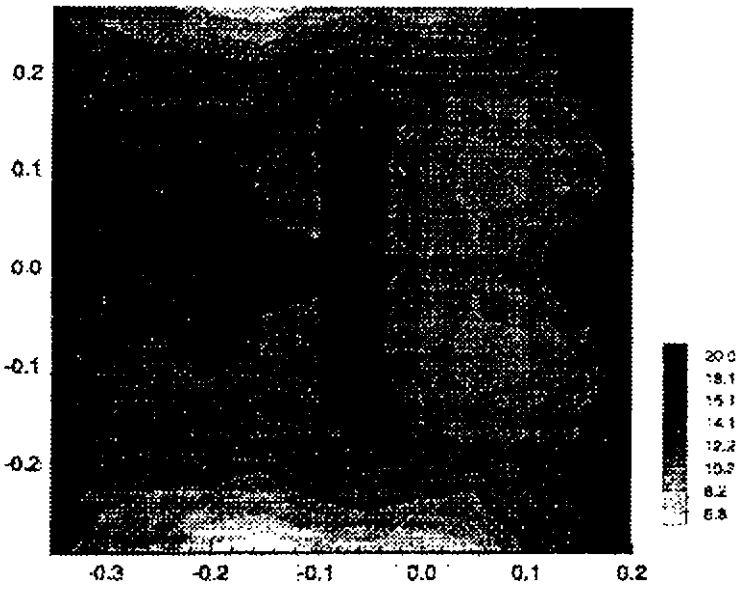

Fig. 18: Image produced by a rough terrain surface in dry sand

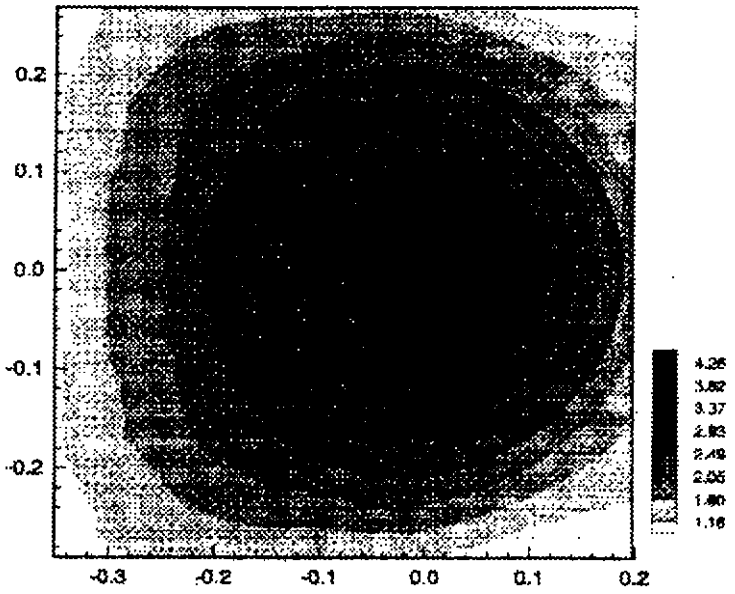

Fig. 19: Image produced by a metallic 10 cm square mine, height 4 cm, buried in dry sand.

5. Conclusions

The efficiency of an electomagnetic imaging principle applied to buried mine searching and identifaction is analysed without worrying much about details of its technical realisation. The usable frequencies for the technique lay in the S-band around 3.5 GHz. This implies that the spatial resolution cannot be much finer than 5 cm. Numerical simulation shows that for favourable soil conditions, e.g. dry sand with a smooth surface, big metallic anti-tank mines and even big plastic mines will actually produce reasonable images with the expected resolution. Pronounced sharp relief-type surface structures, however, may blur the mine images such that only big metallic anti-tank mines could be identified safely under a 10 cm dry sand overburden. In the case of wet clay, mine identification seems to become almost impossible. Attempts to overcome the poor signal to clutter ratio by pattern recognition techniques are hampered by the coarse spatial resolution of the images.

References

1. Habiger K.W., Clifford J.R., Miller R.B., McCullough W.F. (1991) Explosives Detection with Energetic Photons, Nuc. Instrum. and Methods B56/57, 834-838
2. Baum C.E. (1994) Concerning the Identification of Buried Dielectric Targets, Interaction Note 504
3. Graham W.J. (1991) Focused Synthetic Microwave Array for Mine Detection and Imaging, Belvoir Research Report TR-91-001-01
4. Magg M. (1995) Elektromagnetische Feldeinwirkung auf erdüberdeckte Minen, IABG-Report B-TR-M066
5. The MAFIA Collaboration (1994) MAFIA The ECAD System - Manual Version 3.20, CST GmbH, Darmstadt Germany,